



## Submillikelvin Dipolar Molecules in a Radio-Frequency Magneto-Optical Trap

E. B. Norrgard,<sup>1,\*</sup> D. J. McCarron,<sup>1</sup> M. H. Steinecker,<sup>1</sup> M. R. Tarbutt,<sup>2</sup> and D. DeMille<sup>1</sup>

<sup>1</sup>*Department of Physics, Yale University, P.O. Box 208120, New Haven, Connecticut 06520, USA*

<sup>2</sup>*Centre for Cold Matter, Blackett Laboratory, Imperial College London, Prince Consort Road, London SW7 2AZ, United Kingdom*

(Received 1 December 2015; published 10 February 2016)

We demonstrate a scheme for magneto-optically trapping strontium monofluoride (SrF) molecules at temperatures one order of magnitude lower and phase space densities 3 orders of magnitude higher than obtained previously with laser-cooled molecules. In our trap, optical dark states are destabilized by rapidly and synchronously reversing the trapping laser polarizations and the applied magnetic field gradient. The number of molecules and trap lifetime are also significantly improved from previous work by loading the trap with high laser power and then reducing the power for long-term trapping. With this procedure, temperatures as low as 400  $\mu$ K are achieved.

DOI: 10.1103/PhysRevLett.116.063004

Recently, there has been great interest and advancement in producing samples of cold and ultracold ( $T < 1$  mK) polar molecules [1]. The rich internal structure of molecules naturally lends itself to diverse and exciting applications including ultracold chemistry [2], precision measurements [3,4], and quantum simulation [5]. A number of indirect [6–9] and direct [10–13] methods for obtaining ultracold molecules have been demonstrated or are under development. Recently, we have demonstrated use of a magneto-optical trap (MOT) [14,15] to directly cool and trap laser-slowed [16] SrF molecules. A MOT provides simultaneous confinement and cooling, making it the starting point of nearly all experiments with ultracold atoms; the MOT is similarly promising for use with molecules. In this Letter we demonstrate and characterize a scheme for producing a molecular MOT that yields much lower temperature and much higher phase space density than in our previous work.

Most atomic MOTs use a type-I level structure [17] ( $F \rightarrow F' = F + 1$ , where  $F$  is the total angular momentum and the prime indicates the excited state), where all ground states are bright states (here, defined as states addressed by a laser beam that provides a radiative confining force). In molecules, rotational structure requires use of a type-II configuration ( $F \rightarrow F' = F$  or  $F \rightarrow F' = F - 1$ ), which has ground state sublevels not coupled to a confining laser (dark states) for any fixed polarization. The dark state population must be rapidly returned to bright states to allow significant cooling and confinement. Typically, MOTs based on type-II structures are observed to yield weaker confining forces and higher temperatures than those using a type-I structure [18,19].

In this Letter we demonstrate a molecular MOT which destabilizes dark states using time-varying fields. A 3D confining force is produced by diabatically transferring molecules from dark states to bright states; this is accomplished by rapidly and synchronously reversing the  $B$  field and the trapping light polarization [20] [see Fig. 1(a)]. If the

switching is done at a frequency  $f_{\text{MOT}} \gtrsim R_{\text{sc}}$ , where  $R_{\text{sc}}$  is the molecules' photon scattering rate, then the molecules spend a reduced amount of time in dark states and should experience a correspondingly larger force. For a two-level system the maximum value of  $R_{\text{sc}}$  is  $\Gamma/2$ , where the excited state decay rate  $\Gamma$  is typically on the order  $\Gamma \sim 10^7 \text{ s}^{-1}$  [21] ( $\Gamma = 2\pi \times 7$  MHz for SrF). Hence, we refer to the regime  $f_{\text{MOT}} \gtrsim R_{\text{sc}}$  as the radio-frequency (rf) MOT; we distinguish it from the regime  $0 < f_{\text{MOT}} \lesssim R_{\text{sc}}$ , where dark states are destabilized predominantly through other means, which we refer to as the ac MOT. The rf MOT principle was previously used to apply 2D transverse compression on a beam of YO molecules [20], and an ac MOT was used to trap K atoms [22].

In previous work [14,15], we demonstrated MOTs of SrF with static polarizations and  $B$  field. Much of this Letter is devoted to a comparison between these MOTs (which we review here briefly) and the rf MOT. The ground state of SrF has resolved spin-rotation and hyperfine (SR/HF) structure; each of these sublevels must be addressed by

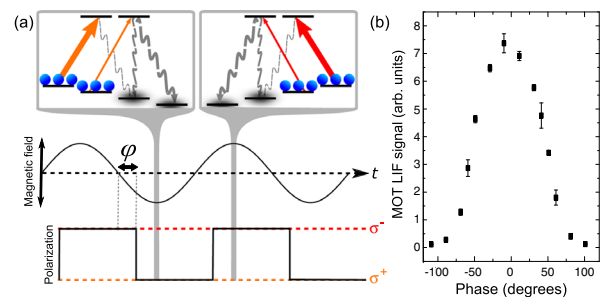


FIG. 1. (a) rf MOT trapping concept. Excitation by a confining laser (the solid arrows) may lead to decay (the dashed arrows) into dark states. The  $B$  field and polarization rapidly reverse such that dark states become bright states; this leads to increased confinement and cooling. (b) LIF from trapped molecules vs relative phase  $\phi$  of the  $B$  field and the laser polarization. Molecules are only trapped for  $|\phi| \lesssim 90^\circ$ .

a separate optical frequency and polarization to achieve reasonable scattering forces. In our original static molecular MOT [14] (referred to here as the dc MOT), the polarizations of the individual frequency components [23] were chosen so that the states Zeeman shifted closest to resonance were bright states. Surprisingly, this scheme does not maximize the restoring force [24], and the confinement was very weak compared to typical atomic MOTs. In subsequent work [15], the polarizations of the components were chosen so that each, treated independently, provided a restoring force [24,25]. This scheme, referred to as the dc\* MOT, gave increased confining forces but significantly higher temperatures. In the rf MOT, the polarizations are the same as in the original dc MOT [23].

In this Letter, we show that the rf MOT makes it possible to obtain much higher phase space density than in the dc or dc\* MOTs: it provides significant confinement and a long lifetime even at low scattering rates, where the lowest temperatures are achieved. Some qualitative explanation of this behavior will be provided by an analytical model of the system.

Much of the experimental scheme has been described elsewhere [14–16,26,27]. Briefly, SrF molecules from a cryogenic beam source [27–29] are slowed by lasers  $\mathcal{L}_{00}$ ,  $\mathcal{L}_{10}$ , and  $\mathcal{L}_{21}$  [16], where  $\mathcal{L}_{vv'}$  denotes a laser tuned to the  $|X^2\Sigma, N=1, v\rangle \rightarrow |A^2\Pi_{1/2}, J=1/2, P=+, v'\rangle$  transition (where  $P$  is the parity). Slow molecules are captured by the MOT, which contains the additional vibrational repump laser  $\mathcal{L}_{32}$ ; due to SrF's highly diagonal matrix of Franck-Condon factors [21], these four lasers allow each molecule to scatter  $\sim 3 \times 10^6$  photons before decaying to uncoupled vibrational levels ( $v \geq 4$ ). Laser  $\mathcal{L}_{00}^{N=3}$  addresses decay to  $|v=0, N=3\rangle$  caused by off-resonant excitation from the optical cycle to  $J'=3/2$  excited states [15]. The SR/HF structure is addressed by adding rf sidebands to each of these MOT lasers. Because one SR/HF level requires a different polarization for trapping [14,24], an additional single-frequency trapping laser  $\mathcal{L}_{00}^\dagger$  with polarization opposite to  $\mathcal{L}_{00}$  and tuned closer than the closest sideband of  $\mathcal{L}_{00}$  to this line allows for a better approximation to the ideal polarization scheme [14,15]. An acousto-optic modulator (AOM) allows the power of main cycling lasers  $\mathcal{L}_{00}$  and  $\mathcal{L}_{00}^\dagger$  to be rapidly changed. Losses from additional optics reduce the maximum  $\mathcal{L}_{00}$  and  $\mathcal{L}_{00}^\dagger$  power to 80 and 30 mW, respectively, compared to 210 and 50 mW in our previous work [14,15]. Trapped molecules are detected by imaging laser-induced fluorescence (LIF) from the main cycling transition onto a CCD camera.

We rapidly switch the polarization of the main cycling lasers using a Pockels cell. The sinusoidally oscillating  $B$ -field gradient is produced by a pair of in-vacuum aluminum nitride (AlN) boards with direct bond copper coils on each side. Variable capacitors external to the vacuum chamber form a parallel  $LC$  tank circuit with the coils resonant at frequency  $f_{\text{MOT}}$ , and impedance match

to  $50\Omega$ . Adjusting the capacitors allows  $f_{\text{MOT}}$  to be easily varied from dc to 3 MHz (limited by the coils' self-capacitance) with loaded  $Q \approx 50$  for  $f_{\text{MOT}} > 0.5$  MHz.

A peak current of 5 A is required to produce the optimum rms axial  $B$ -field gradient of 9 G/cm. Given our coil inductance of 40  $\mu\text{H}$ , this requires a peak voltage  $V_{\text{pk}} = 4$  kV when  $f_{\text{MOT}} = 3$  MHz. We take care to minimize the  $\mathcal{E}$  field produced by this voltage drop: the four coils (one on each side of each board) are wired in series, with the coils on the bottom board ordered first and last and the top board coils intermediate, leading to equal average potentials on the two boards. Nevertheless, the residual  $\mathcal{E}$  field has observable effects on the trap lifetime (discussed below and in the Supplemental Material [30]).

Defining the time of the laser ablation pulse that initiates a molecular beam pulse as  $t = 0$ , we find the maximum population occurs at  $t \approx 70$  ms. Figure 1(b) shows the LIF recorded for a 60 ms exposure starting at  $t = 70$  ms as a function of the relative phase  $\phi$  of the  $B$ -field gradient and laser polarization. As expected, the signal is greatest when  $\phi \approx 0$  and vanishes for  $|\phi| \gtrsim 90^\circ$ . This clearly demonstrates trapping via the rf MOT mechanism. For optimal trap loading,  $\mathcal{L}_{00}$  and  $\mathcal{L}_{00}^\dagger$  are detuned from a nominal resonant frequency (the frequency which produces maximum LIF when the lasers are applied orthogonal to the molecular beam in zero  $B$  field) by about  $-9$  and  $-6$  MHz, respectively.

The number of trapped molecules is determined from  $R_{\text{sc}}$ , MOT lifetime  $\tau_{\text{MOT}}$ , and integrated LIF intensity from a 60 ms camera exposure as in Ref. [14]. The peak trap population vs  $\mathcal{L}_{00}$  power is plotted in Fig. 2(a) (throughout this Letter, whenever  $\mathcal{L}_{00}$  varies from full power, it is implicit that the  $\mathcal{L}_{00}^\dagger$  power is changed by a proportional amount using the AOM). The number of trapped molecules grows monotonically with the laser power. Under optimal conditions,  $> 2000$  molecules are loaded into the rf MOT at full power, and there is no clear dependence on  $f_{\text{MOT}}$  in the range 1.23–2.40 MHz. Operation at  $f_{\text{MOT}} = 111$  kHz was much more sensitive to MOT beam alignment than for  $f_{\text{MOT}} > 1$  MHz, so we speculate that the slightly lower number loaded may be attributed to drifting beam pointing. We find that the rf MOT loads  $\sim 3$  times more molecules than the dc\* MOT.

The photon scattering rate  $R_{\text{sc}}$  [plotted vs  $\mathcal{L}_{00}$  power in Fig. 2(b)] is determined by comparing the measured decay rate of the LIF signal when  $\mathcal{L}_{32}$  is rapidly shuttered vs when  $\mathcal{L}_{32}$  is present, given the known branching ratio into  $v = 3$  ( $\approx 9.6 \times 10^{-6}$  [33,34]). A simple analytical rate model predicts that the steady-state scattering rate in the MOT has the same form as a two-level system [4]:

$$R_{\text{sc}} = \frac{\Gamma_{\text{eff}}}{2} \frac{I_{00}/I_{\text{sat,eff}}}{1 + I_{00}/I_{\text{sat,eff}} + 4\Delta^2/\Gamma^2}. \quad (1)$$

Here,  $I_{00}$  is the  $\mathcal{L}_{00}$  intensity,  $I_{\text{sat,eff}}$  is an effective saturation intensity,  $\Gamma_{\text{eff}}/2$  is the maximum scattering rate, and  $\Delta$  is

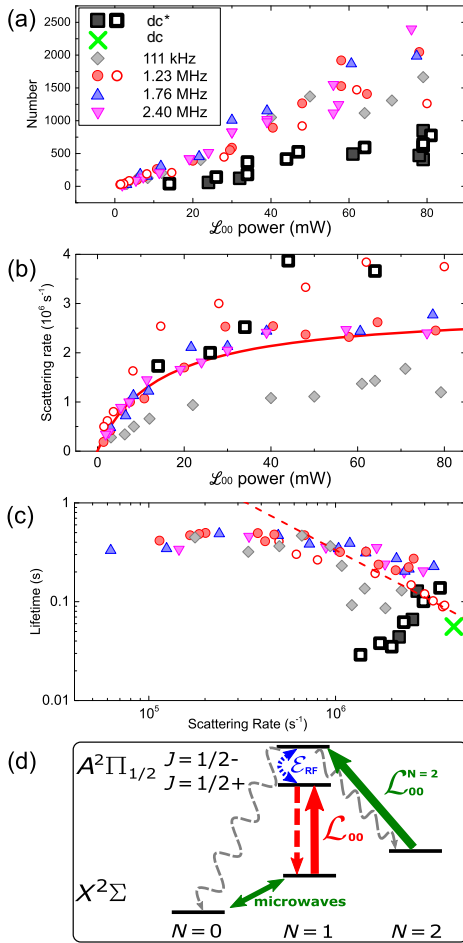


FIG. 2. Filled markers, microwaves applied; open markers, without. (a) Number of molecules loaded into the MOT vs  $\mathcal{L}_{00}$  power. The number increases with increasing  $\mathcal{L}_{00}$  power in all cases. (b) Scattering rate vs  $\mathcal{L}_{00}$  power. The solid line is a fit of the model described in the text to  $f_{\text{MOT}} = 1.23$  MHz data, with  $\Delta$  set to  $-2\pi \times 9$  MHz, and fit values  $\Gamma_{\text{eff}} = 2\pi \times 1.0(1)$  MHz and  $p_{\text{sat}} = 1.9(3)$  mW.  $R_{\text{sc}}$  is lower for  $f_{\text{MOT}} = 111$  kHz than for  $f_{\text{MOT}} > 1$  MHz.  $R_{\text{sc}}$  increases in the absence of repump microwaves by  $\sim 40\%$ . (c) Trap lifetime  $\tau_{\text{MOT}}$  vs  $R_{\text{sc}}$ .  $\tau_{\text{MOT}}$  as long as 500 ms are achieved for low  $R_{\text{sc}}$ 's in the rf MOT. For higher  $R_{\text{sc}}$ 's,  $\tau_{\text{MOT}} \propto 1/R_{\text{sc}}$  (the dashed line is a  $1/R_{\text{sc}}$  trend line), and  $\tau_{\text{MOT}}$  is much shorter in the absence of repump microwaves. For the dc\* MOT,  $\tau_{\text{MOT}}$  decreases for lower  $R_{\text{sc}}$ 's. (d) Parity mixing (the curved blue line) due to the coil-induced electric field  $\mathcal{E}_{\text{rf}}$  causes loss (the wiggly grey lines) from the main cycling transition (the vertical red lines), which is repumped via  $\mathcal{L}_{00}^{N=2}$  and resonant microwaves (the diagonal green lines).

the detuning from resonance. The model is discussed in more detail in the Supplemental Material [35], where expressions for  $\Gamma_{\text{eff}}$  and  $I_{\text{sat,eff}}$  in terms of known molecular parameters are also given. These expressions predict  $\Gamma_{\text{eff}} = 2\pi \times 1.7$  MHz and  $I_{\text{sat,eff}}$  corresponding to saturation power  $p_{\text{sat}} = 2.6$  mW for our 7 mm  $1/e^2$  radius MOT beams. The solid line in Fig. 2(b) shows a fit of Eq. (1) to the data for  $f_{\text{MOT}} = 1.23$  MHz. We fix  $\Delta = -2\pi \times 9$  MHz

and find the best fit parameters to be  $\Gamma_{\text{eff}} = 2\pi \times 1.0(1)$  MHz, about 40% smaller than the predicted value, and  $p_{\text{sat}} = 1.9(3)$  mW, about 25% smaller than predicted. We see that, despite the complexity of the MOT, this simple model predicts the scattering rate quite well. However, we are unable to quantitatively explain the much lower  $R_{\text{sc}}$  observed for  $f_{\text{MOT}} = 111$  kHz, which is well into the ac MOT regime for all but the very lowest  $R_{\text{sc}}$  explored here.

In simplifying limits, other well-known equations approximating trap properties, such as the spring constant  $\kappa$  and temperature  $T$ , may be expressed in terms of either  $R_{\text{sc}}$  or  $I_{00}/I_{\text{sat,eff}}$ . Because  $R_{\text{sc}}$  may be easily measured in the lab and the expected dependence of the trap properties is simpler when expressed in terms of  $R_{\text{sc}}$ , we choose to plot the remainder of our data as a function of  $R_{\text{sc}}$ , rather than power or intensity.

The MOT lifetime  $\tau_{\text{MOT}}$  is measured by monitoring LIF as a function of time [see Fig. 2(c)]. Radio-frequency  $\mathcal{E}$  fields caused by the large rf voltage applied to the MOT coils mix the excited  $|J = 1/2, P = \pm\rangle$  states and lead to unwanted branching to the  $N = 0, 2$  ground states. In the absence of a mechanism to couple these states to the main cycling transition, this leads to relatively short trap lifetimes. As shown in Fig. 2(d), we mitigate this loss with a  $\sim 5$  mW laser  $\mathcal{L}_{00}^{N=2}$  (which pumps  $N = 2$  into  $N = 0$  via  $|A^2\Pi_{1/2}, J = 1/2, P = -\rangle$ ) plus microwaves resonant with both  $|N = 0, J = 1/2, F = 0, 1\rangle \leftrightarrow |N = 1, J = 1/2, F = 1, 0\rangle$  transitions. For intermediate scattering rates [ $R_{\text{sc}} \sim (2-8) \times 10^5 \text{ s}^{-1}$ ] with these additional fields applied,  $\tau_{\text{MOT}}$  is independent of  $f_{\text{MOT}}$  and is especially long ( $\sim 500$  ms). Despite decreasing the maximum  $R_{\text{sc}}$  by  $\sim 40\%$  [roughly the expected amount due to additional levels coupled to the cycling transition [35]; see Fig. 2(b)], microwaves are found to not dramatically affect other trap properties. For the highest scattering rates, the trap loss rate  $R_{\text{loss}} = 1/\tau_{\text{MOT}}$  is proportional to  $R_{\text{sc}}$ , indicative of a scattering-related loss mechanism whose origin is not currently understood. In contrast to the rf MOT, the dc\* MOT lifetime decreases sharply for lower scattering rates, rendering it incapable of trapping at  $R_{\text{sc}} \lesssim 10^6 \text{ s}^{-1}$ . The dc MOT was found to be even more short lived at any reduced power; the single points in Figs. 2 and 3 were taken from Ref. [14].

While the MOT loads the most molecules at full laser power, we observe that other trap properties improve as the power of the main cycling lasers is reduced. We therefore employ a loading stage at full laser power to capture the largest possible sample, then reduce the  $\mathcal{L}_{00}$  and  $\mathcal{L}_{00}^\dagger$  powers. By linearly decreasing the power from its full initial value to a lower final value over a time  $t_{\text{ramp}} > 30$  ms, the fraction of trapped molecules remaining is near unity, even when the power is reduced by 99.5%. For all data in Fig. 3, we use  $t_{\text{ramp}} = 50$  ms.

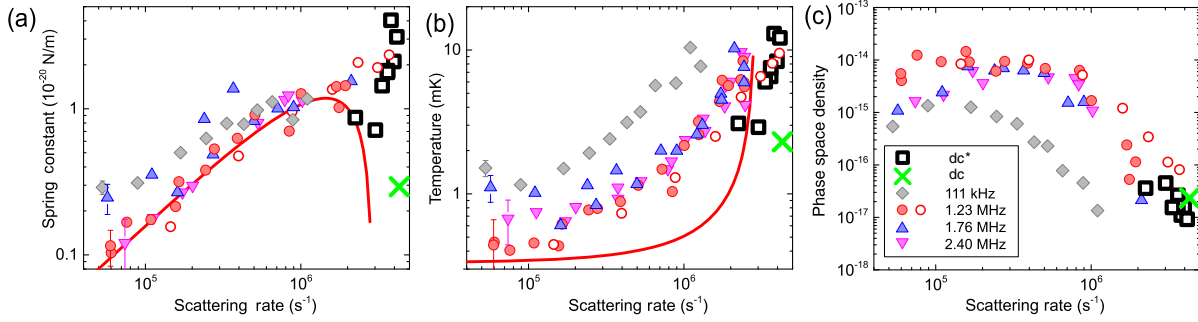


FIG. 3. Filled symbols, microwaves applied; open symbols, without; red line, analytical model fit to  $f_{\text{MOT}} = 1.23$  MHz data. Measured (a) spring constant  $\bar{\kappa}$  and (b) temperature  $\bar{T}$  vs scattering rate  $R_{sc}$ . The maximum  $\bar{\kappa}$  for the dc\* MOT is  $\sim 2$  times that of the rf MOT, but it decreases much more rapidly for lower  $R_{sc}$ . The analytical model, with  $\Gamma_{\text{eff}}$  set to the fit value from  $R_{sc}$  vs  $I_{00}$ , and  $B$ -field gradient  $\partial B_z/\partial z$  and detuning  $\Delta$  set to experimental values, has  $\mu_{\text{eff}}$  as the only free parameter.  $\bar{T}$  decreases with falling  $R_{sc}$ , but at a slower rate than predicted by the analytical model with no free parameters.  $\bar{T}$  is lower for  $f_{\text{MOT}} > 1$  MHz than for  $f_{\text{MOT}} = 111$  kHz. The model correctly predicts  $\bar{T} \sim T_D$  for a low  $R_{sc}$ . The spread in values for a given MOT configuration is indicative of variations between measurements made on the same day, while the representative error bars are standard errors of measurements taken on multiple days under similar conditions. (c) Phase space density  $\rho$  vs  $R_{sc}$  after a linear power ramp from full power. Ramping increases  $\rho$  by up to 2.5 orders of magnitude in the rf MOT. In the dc\* MOT,  $\rho$  increases only slightly when  $R_{sc}$  is lowered.

The radial and axial temperatures  $T_\rho$  and  $T_z$  and spring constants  $\kappa_\rho$  and  $\kappa_z$  are measured by observing the free expansion of molecules released from the MOT. The trapping potential is removed by turning off the  $B$  field and the main cycling lasers for a variable duration  $t_{\text{TOF}}$ , during which time the molecules ballistically expand. The main cycling lasers are then restored, and the molecule cloud is imaged for 2 ms.

The geometric mean spring constant  $\bar{\kappa} \equiv \kappa_\rho^{2/3} \kappa_z^{1/3}$  is shown as a function of  $R_{sc}$  in Fig. 3(a). While  $\bar{\kappa}$  remains significant even for a low  $R_{sc}$  in the rf MOT, it falls dramatically with a decreasing  $R_{sc}$  in the dc\* MOT. The spread in  $\bar{\kappa}$  for different  $f_{\text{MOT}}$ 's at low  $R_{sc}$  is typical of day-to-day fluctuations in  $\bar{\kappa}$  due to drifting alignment. In the analytical model detailed in the Supplemental Material [35],  $\bar{\kappa}$  is related to  $R_{sc}$  by

$$\bar{\kappa} = -\frac{8\Delta k R_{sc} (1 - 2R_{sc}/\Gamma_{\text{eff}}) \mu_{\text{eff}} (\partial B_z/\partial z)}{3 \times 4^{1/3} \Gamma^2 (1 + 4\Delta^2/\Gamma^2)}, \quad (2)$$

where  $k$  is the wave number,  $\partial B_z/\partial z$  is the axial  $B$ -field gradient, and  $\mu_{\text{eff}}$  is an effective magnetic moment. The solid line in Fig. 3(a) shows a fit of Eq. (2) to the data with  $f_{\text{MOT}} = 1.23$  MHz. In this fit, we fix  $\Gamma_{\text{eff}}$  to the value found above and use experimental values  $\partial B_z/\partial z = 9$  G/cm and  $\Delta = -2\pi \times 9$  MHz, leaving  $\mu_{\text{eff}}$  as the only free parameter. The best fit gives  $\mu_{\text{eff}} = 0.32(1)\mu_B$ . This is not too different from the level-averaged value  $\langle |\mu| \rangle = \sum_i^n |\mu_i|/n = 0.49\mu_B$ , where  $\mu_i$  is the magnetic moment in the weak-field limit of Zeeman sublevel  $i$ , and the sum is over the sublevels of ( $v = 0, N = 1$ ). We see that the trapping forces in the rf MOT are reasonably well described by this simple model.

The geometric mean temperature  $\bar{T} \equiv T_\rho^{2/3} T_z^{1/3}$  is shown vs  $R_{sc}$  in Fig. 3(b). There is little frequency dependence to  $\bar{T}$  for  $f_{\text{MOT}} > 1$  MHz, while the 111 kHz ac MOT is substantially hotter. The temperature decreases with decreasing scattering rate for all  $f_{\text{MOT}}$ 's, qualitatively matching the expected behavior for Doppler cooling [35]:

$$T = -\frac{\hbar\Gamma^2 (1 + 4\Delta^2/\Gamma^2)}{8k_B\Delta (1 - 2R_{sc}/\Gamma_{\text{eff}})}. \quad (3)$$

The solid line in Fig. 3(b) shows this predicted behavior, with  $\Gamma_{\text{eff}}$  and  $\Delta$  fixed as above. There are no free parameters. At low  $R_{sc}$ 's, we measure  $\bar{T}$  as low as 400  $\mu\text{K}$ , fairly close to the 245  $\mu\text{K}$  predicted by Eq. (3) (for SrF, the minimum Doppler cooling temperature  $T_D = 160$   $\mu\text{K}$  would be expected for  $\Delta = -\Gamma/2 \approx -2\pi \times 3$  MHz). Cooling to near the temperature predicted by simple Doppler cooling theory at low intensities has been observed in systems where sub-Doppler cooling mechanisms are weak or absent [37,38]. However, we observe that  $\bar{T}$  increases far more rapidly with an increasing  $R_{sc}$  than suggested by Eq. (3). Similar behavior has been observed in Sr [37] and is not well understood, but this may be due to stimulated-force heating effects [39–41].

Figure 3(c) shows the phase space density  $\rho$  vs  $R_{sc}$ , inferred from  $\bar{\kappa}$ ,  $\bar{T}$ , and molecule number. At the highest scattering rates,  $\rho$  is similar for the dc, dc\*, and rf MOTs. Lowering  $R_{sc}$  increases  $\rho$  by  $\sim 2.5$  orders of magnitude in the rf MOT, with  $\rho$  roughly constant over the range  $R_{sc} \sim 10^5$ – $10^6$   $s^{-1}$ . The hotter  $f_{\text{MOT}} = 111$  kHz ac MOT has  $\rho \sim 10$  times lower than rf MOTs with  $f_{\text{MOT}} > 1$  MHz. In the dc\* MOT,  $\rho$  increases only modestly at lower  $R_{sc}$ 's.

The dc and dc\* MOTs have polarization schemes intended to repump dark states with orthogonal and

anticonfining MOT laser beams [15], while in the rf MOT the laser polarizations and the  $B$  field are reversed before this repumping occurs. The rf MOT was therefore expected to have a larger value of  $\bar{\kappa}$  than the dc\* MOT. However, we find them to be comparable at high values of  $R_{sc}$  [see Fig. 3(a)]. Recently, it was shown that the close spacing of the SR/HF levels in SrF leads to a dual-frequency mechanism, where two oppositely polarized frequency components addressing the same transition can deplete dark states [23,25]. A state which is dark to one component is bright to the oppositely polarized component, so molecules can scatter continuously from a confining beam, with a preference for that beam dictated by the Zeeman shift. This mechanism is responsible for the majority of the confinement in the dc\* MOT [25]. In the rf MOT, dark states in all SR/HF levels are automatically converted to bright states by the time-varying fields.

While the rf MOT was not found to provide a larger restoring force than the dc\* MOT, its ability to provide significant confinement even at greatly reduced power is extremely useful. By loading at high power and ramping to low power, we produce a sample of 2000 molecules with 0.5 s lifetime at 400  $\mu$ K with density  $6 \times 10^4 \text{ cm}^{-3}$  and phase space density  $1.5 \times 10^{-14}$ . These correspond to factors of 3, 4, 6, 15, and 1000 improvement, respectively, over previous molecular MOTs [14,15]. There are promising ideas for delivering much larger numbers of slow molecules for loading into a rf MOT, such as microwave guiding [42], bichromatic force slowing [43], or (for molecules with a  $^1\Sigma$  ground state, where the magnetic moment is negligible) a Zeeman slower [34,44].

The temperatures reported here,  $\approx 3T_D$ , are sufficiently cold to have a broad impact on the field. For example, molecular fountains could be constructed to offer long interaction times for precision measurements [4]. Additionally, 400  $\mu$ K molecules could be magnetically trapped with standard techniques. Cotrapping with an ultracold atom would allow study of atom-molecule collisions and potentially sympathetic cooling to yet lower temperatures [45–47].

The authors acknowledge E. R. Edwards and N. R. Hutzler for their input on rf MOT coil design and financial support from ARO and ARO (MURI). E. B. N. acknowledges funding from the NSF GRFP.

*Note added in proof.*—Similar results on direct cooling of molecules to submillikelvin temperatures using optoelectrical Sisyphus cooling are reported in Ref. [48].

---

\*Corresponding author.  
eric.norrgard@yale.edu

[1] L. Carr, D. DeMille, R. Krems, and J. Ye, Cold and ultracold molecules: Science, technology and applications, *New J. Phys.* **11**, 055049 (2009).

- [2] R. V. Krems, Cold controlled chemistry, *Phys. Chem. Chem. Phys.* **10**, 4079 (2008).
- [3] L. R. Hunter, S. K. Peck, A. S. Greenspon, S. S. Alam, and D. DeMille, Prospects for laser cooling TIF, *Phys. Rev. A* **85**, 012511 (2012).
- [4] M. R. Tarbutt, B. E. Sauer, J. J. Hudson, and E. A. Hinds, Design for a fountain of YbF molecules to measure the electron's electric dipole moment, *New J. Phys.* **15**, 053034 (2013).
- [5] A. Micheli, G. K. Brennen, and P. Zoller, A toolbox for lattice-spin models with polar molecules, *Nat. Phys.* **2**, 341 (2006).
- [6] K. Ni, S. Ospelkaus, M. H. G. de Miranda, A. Pe'er, B. Neyenhuis, J. J. Zirbel, S. Kotochigova, P. S. Julienne, D. S. Jin, and J. Ye, A high phase-space-density gas of polar molecules, *Science* **322**, 231 (2008).
- [7] J. G. Danzl, M. J. Mark, E. Haller, M. Gustavsson, R. Hart, J. Aldegunde, J. Hutson, and H.-C. Nägerl, An ultracold high-density sample of rovibronic ground-state molecules in an optical lattice, *Nat. Phys.* **6**, 265 (2010).
- [8] K. Aikawa, D. Akamatsu, M. Hayashi, K. Oasa, J. Kobayashi, P. Naidon, T. Kishimoto, M. Ueda, and S. Inouye, Coherent Transfer of Photoassociated Molecules into the Rovibrational Ground State, *Phys. Rev. Lett.* **105**, 203001 (2010).
- [9] T. Shimasaki, M. Bellos, C. D. Bruzewicz, Z. Lasner, and D. DeMille, Production of rovibronic-ground-state RbCs molecules via two-photon-cascade decay, *Phys. Rev. A* **91**, 021401 (2015).
- [10] M. Zeppenfeld, B. G. U. Englert, R. Glöckner, A. Prehn, M. Mielenz, C. Sommer, L. D. van Buuren, M. Motsch, and G. Rempe, Sisyphus cooling of electrically trapped polyatomic molecules, *Nature (London)* **491**, 570 (2012).
- [11] B. K. Stuhl, M. T. Hummon, M. Yeo, G. Quémener, J. L. Bohn, and J. Ye, Evaporative cooling of the dipolar hydroxyl radical, *Nature (London)* **492**, 396 (2012).
- [12] H.-I. Lu, I. Kozyryev, B. Hemmerling, J. Piskorski, and J. M. Doyle, Magnetic Trapping of Molecules via Optical Loading and Magnetic Slowing, *Phys. Rev. Lett.* **112**, 113006 (2014).
- [13] V. Zhelyazkova, A. Cournol, T. E. Wall, A. Matsushima, J. J. Hudson, E. A. Hinds, M. R. Tarbutt, and B. E. Sauer, Laser cooling and slowing of CaF molecules, *Phys. Rev. A* **89**, 053416 (2014).
- [14] J. F. Barry, D. J. McCarron, E. N. Norrgard, M. H. Steinecker, and D. DeMille, Magneto-optical trapping of a diatomic molecule, *Nature (London)* **512**, 286 (2014).
- [15] D. J. McCarron, E. B. Norrgard, M. H. Steinecker, and D. DeMille, Improved magneto-optical trapping of a diatomic molecule, *New J. Phys.* **17**, 035014 (2015).
- [16] J. F. Barry, E. S. Shuman, E. B. Norrgard, and D. DeMille, Laser Radiation Pressure Slowing of a Molecular Beam, *Phys. Rev. Lett.* **108**, 103002 (2012).
- [17] M. Prentiss, A. Cable, J. E. Bjorkholm, S. Chu, E. L. Raab, and D. E. Pritchard, Atomic-density-dependent losses in an optical trap, *Opt. Lett.* **13**, 452 (1988).
- [18] A. M. L. Oien, I. T. McKinnie, P. J. Manson, W. J. Sandle, and D. M. Warrington, Cooling mechanisms in the sodium type-II magneto-optical trap, *Phys. Rev. A* **55**, 4621 (1997).

- [19] V. B. Tiwari, S. Singh, H. S. Rawat, and S. C. Mehendale, Cooling and trapping of  $^{85}\text{Rb}$  atoms in the ground hyperfine  $F = 2$  state, *Phys. Rev. A* **78**, 063421 (2008).
- [20] M. T. Hummon, M. Yeo, B. K. Stuhl, A. L. Collopy, Y. Xia, and J. Ye, 2D Magneto-Optical Trapping of Diatomic Molecules, *Phys. Rev. Lett.* **110**, 143001 (2013).
- [21] M. D. Di Rosa, Laser-cooling molecules, *Eur. Phys. J. D* **31**, 395 (2004).
- [22] M. Harvey and A. J. Murray, Cold Atom Trap with Zero Residual Magnetic Field: The ac Magneto-Optical Trap, *Phys. Rev. Lett.* **101**, 173201 (2008).
- [23] See Supplemental Material, Fig. 1 at <http://link.aps.org/supplemental/10.1103/PhysRevLett.116.063004> for the frequency and polarization scheme.
- [24] M. R. Tarbutt, Magneto-optical trapping forces for atoms and molecules with complex level structures, *New J. Phys.* **17**, 015007 (2015).
- [25] M. R. Tarbutt and T. C. Steimle, Modeling magneto-optical trapping of CaF molecules, *Phys. Rev. A* **92**, 053401 (2015).
- [26] E. S. Shuman, J. F. Barry, and D. DeMille, Laser cooling of a diatomic molecule, *Nature (London)* **467**, 820 (2010).
- [27] J. F. Barry, E. S. Shuman, and D. DeMille, A bright, slow cryogenic molecular beam source for free radicals, *Phys. Chem. Chem. Phys.* **13**, 18936 (2011).
- [28] D. Patterson and J. M. Doyle, Bright, guided molecular beam with hydrodynamic enhancement, *J. Chem. Phys.* **126**, 154307 (2007).
- [29] N. R. Hutzler, H.-I. Lu, and J. M. Doyle, The buffer gas beam: An intense, cold, and slow source for atoms and molecules, *Chem. Rev.* **112**, 4803 (2012).
- [30] See Supplemental Material at <http://link.aps.org/supplemental/10.1103/PhysRevLett.116.063004>, which includes Refs. [31,32], for further details on the effects of rf  $\mathcal{E}$  fields.
- [31] P. M. Sheridan, J.-G. Wang, M. J. Dick, and P. F. Bernath, Optical-Optical double resonance spectroscopy of the  $C^2\Pi - A^2\Pi$  and  $D^2\Sigma^+ - A^2\Pi$  transitions of SrF, *J. Phys. Chem. A* **113**, 13383 (2009).
- [32] J. Kändler, T. Martell, and W. E. Ernst, Electric dipole moments and hyperfine structure of SrF  $A^2\Pi$  and  $B^2\Sigma^+$ , *Chem. Phys. Lett.* **155**, 470 (1989).
- [33] F. Stienkemeier, Ph.D. thesis, Universität Bielefeld, 1993.
- [34] J. F. Barry, Ph.D. thesis, Yale University, 2013.
- [35] See Supplemental Material at <http://link.aps.org/supplemental/10.1103/PhysRevLett.116.063004>, which includes Ref. [36], for additional details on the analytical model.
- [36] P. D. Lett, W. D. Phillips, S. L. Rolston, C. E. Tanner, R. N. Watts, and C. I. Westbrook, Optical molasses, *J. Opt. Soc. Am. B* **6**, 2084 (1989).
- [37] X. Xu, T. H. Loftus, J. L. Hall, A. Gallagher, and J. Ye, Cooling and trapping of atomic strontium, *J. Opt. Soc. Am. B* **20**, 968 (2003).
- [38] R. Chang, A. L. Hoendervanger, Q. Bouton, Y. Fang, T. Klafka, K. Audo, A. Aspect, C. I. Westbrook, and D. Clément, Three-dimensional laser cooling at the Doppler limit, *Phys. Rev. A* **90**, 063407 (2014).
- [39] J. P. Gordon and A. Ashkin, Motion of atoms in a radiation trap, *Phys. Rev. A* **21**, 1606 (1980).
- [40] J. Dalibard and C. Cohen-Tannoudji, Dressed-atom approach to atomic motion in laser light: The dipole force revisited, *J. Opt. Soc. Am. B* **2**, 1707 (1985).
- [41] P. L. Gould, P. J. Martin, G. A. Ruff, R. E. Stoner, J.-L. Picqué, and D. E. Pritchard, Momentum transfer to atoms by a standing light wave: Transition from diffraction to diffusion, *Phys. Rev. A* **43**, 585 (1991).
- [42] D. DeMille, J. F. Barry, E. R. Edwards, E. B. Norrgard, and M. H. Steinecker, On the transverse confinement of radiatively slowed molecular beams, *Mol. Phys.* **111**, 1805 (2013).
- [43] M. A. Chiedo and E. E. Eyler, Prospects for rapid deceleration of small molecules by optical bichromatic forces, *Phys. Rev. A* **84**, 063401 (2011).
- [44] R. J. Hendricks, D. A. Holland, S. Truppe, B. E. Sauer, and M. Tarbutt, Vibrational branching ratios and hyperfine structure of  $^{11}\text{BH}$  and its suitability for laser cooling, *Front. Phys.* **2**, 51 (2014).
- [45] J. Lim, M. D. Frye, J. M. Hutson, and M. R. Tarbutt, Modeling sympathetic cooling of molecules by ultracold atoms, *Phys. Rev. A* **92**, 053419 (2015).
- [46] M. Lara, J. L. Bohn, D. Potter, P. Soldán, and J. M. Hutson, Ultracold Rb-OH Collisions and Prospects for Sympathetic Cooling, *Phys. Rev. Lett.* **97**, 183201 (2006).
- [47] P. Soldán, P. S. Żuchowski, and J. M. Hutson, Prospects for sympathetic cooling of polar molecules: NH with alkali-metal and alkaline-earth atoms—a new hope, *Faraday Discuss.* **142**, 191 (2009).
- [48] A. Prehn, M. Ibrügger, R. Glockner, G. Rempe, and M. Zeppenfeld, following Letter, Optoelectrical Cooling of Polar Molecules to Submillikelvin Temperatures, *Phys. Rev. Lett.* **116**, 063005 (2016).